Quantum images in double-slit experiments with spontaneous down-conversion light

G. A. Barbosa*

Conselho Nacional de Desenvolvimento Cientifico e Technologico, Departamento de Física–Instituto de Ciências Exatas–Universidade Federal de Minas Gerais, Caixa Postal 702, Belo Horizonte 30161-970, Minas Gerais, Brazil

(Received 3 November 1995; revised manuscript received 10 July 1996)

A fourth-order correlation function in the $\{\mathbf{r}\}$ space is developed and applied to double-slit experiments with spontaneous down-conversion light. The predicted coincidence patterns and corresponding degrees of visibility agree with the experimental results. The van Cittert–Zernike theorem is extended to coincidence experiments. [S1050-2947(96)00911-0]

PACS number(s): 42.50.Dv, 42.50.Ar, 42.30.Va

I. INTRODUCTION

Beyond the traditional concept of *intensity* images crystalized in our minds by direct sensorial experience, another type of image has been revealed in recent experiments. These images appear in fourth-order correlation functions of special electromagnetic fields, even when no intensity image is presented by the second-order correlation function. Of course, an electromagnetic field is completely characterized by the knowledge of its correlation functions in all orders, and these fourth-order images indicate an open field to be explored.

This work deals with patterns seen when a beam of *spontaneous* down-converted light illuminates a double slit (Young) and its conjugated beam is scanned spatially searching for correlations or, conversely, the conjugate detector is kept fixed and a Young *coincidence* pattern appears on scanning behind the double-slit arrangement. It is well known that down-converted conjugated beams (''signal'' and ''idler'') have spatial correlations [1] and particularly a strong number correlation between signal and idler photons. The Young slit arrangement provides an extension of this point-point correlation using an *interference* pattern.

The spontaneous parametric down-conversion luminescence [1] is a nonlinear second-order process, where one photon from a pump laser at frequency ω_p, usually an UV frequency for higher efficiency, excites a nonlinear crystal nonresonantly, in a virtual process. The crystal decays, within an infinitesimally short time from the excitation, into two simultaneous photons of energies ω_s and ω_i.

Although the pumping laser photons may be highly coherent, neither signal *nor* idler down-converted photons carry this coherence. The *temporal* and *spatial* correlations between the signal and idler photons are established at the photon source by the energy and phase matching (momentum) constraints; these correlations propagate with the down-converted beams away from the crystal.

An initial experiment, by Ribeiro *et al.* [2] (see Fig. 1), was performed with Young slits, demonstrating that coincidence interference fringes could be obtained when scanning transversally the signal detector behind the slits, even when the coherence area for the field was smaller than the slit separation. The degree of visibility obtained was shown to be controlled *nonlocally* by varying the pinhole size in the idler beam. While a qualitative explanation for the phenomenon was presented, an adequate theory was not developed.

In another experiment, by Shih *et al.* [3], with a similar setup, they show that coincidence fringes could also be obtained scanning the idler beam, although the slit was placed in the signal detector. The obtained fringes were called ''ghost'' fringes. A very simple interpretation was given using the transverse momentum conservation and geometrical considerations. That work also exemplified the known point-point correlation between signal and idler by placing an object in the signal beam and reproducing it by scanning the idler beam; they coined the name ''quantum-fax'' to this information transfer.

The use of conjugate beams as potential quantum-mechanically protected information carriers has been discussed by several authors (see, for example, [4]). Although interesting schemes can be developed aimed at communica-

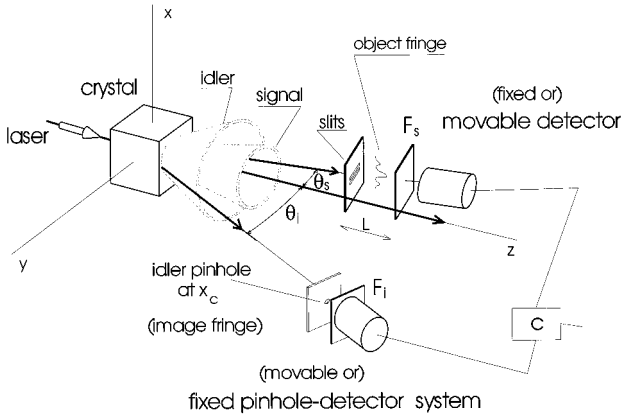

FIG. 1. Simplified setup: a laser of angular frequency ω_p and wave vector $\mathbf{k}_p$ excite a nonlinear crystal. Conjugate ''signal'' and ''idler'' photons are spontaneously emitted, such that $\mathbf{k}_p n_p \simeq \mathbf{k}_s n_s + \mathbf{k}_i n_i$ and $\omega_p = \omega_s + \omega_i$. Interference filters F_s and F_i are placed just before the detectors. θ_s and θ_i are the polar angles between each conjugated beam and the pump beam. An ''object'' fringe is seen scanning the signal detector vertically (the weak divergence condition) with a fixed idler detector. The ''image'' fringe is obtained with a fixed signal detector and scanning the idler pinhole-detector system. For points near the (y,z) plane, $\mathbf{r}_i = (x_c + \rho\ \sin\varphi)\hat{\mathbf{i}} + (r_{i0}\sin\theta_{i0} + \rho\cos\varphi)\hat{\mathbf{j}} + (r_{i0}\cos\theta_{i0} - \rho\sin\varphi)\hat{\mathbf{k}}$ and the signal slits are at $\mathbf{r}_1 = d/2\hat{\mathbf{i}}$ and $\mathbf{r}_2 = -d/2\hat{\mathbf{i}}$.

*Electronic address: gbarbosa@fis.ufal.br

 © 1996 The American Physical Society

tion ends or the study of Einstein-Podolsky-Rosen pairs [5], the understanding of the basic transverse correlations present in the down-converted field cannot be underestimated, as demonstrated by the experiments described above.

Although intuitive and qualitative explanations have been put forth, a multimode quantum theory has to be applied to a complete understanding of these phenomena. The basic multimode theory perfected by Mandel and co-workers [6] has been successfully applied to several experiments exploring the *longitudinal* coherence properties of the conjugate beams. However, only recently have the *transverse* correlation properties of these beams started to be studied (see, for example, [7–9]). The present work applies Mandel's theory to explore these *transverse* properties and to generate fourth-order correlation functions in the $\{\mathbf{r}\}$ space.

This work shows that although a frequency divergence $\Delta\omega$ is always present around a given direction in the down-conversion, the fundamental divergence responsible for these transverse correlations is an angular divergence in wave vectors, at *constant* frequency. Frequency and angular divergences will be considered, but special emphasis will be given to the *multimode* (in the wave vector) *monochromatic* aspect.[1]

Throughout this work, the name *object pattern* will be applied to the coincidence pattern detected by scanning behind the double slit in the signal beam, while *image pattern* will designate the coincidence pattern detected by scanning the idler detector. Object and image patterns, or ''quantum images,'' are simultaneously generated in this calculation, in agreement with the experimental results. The dependence on all experimental variables such as distances involved, slits, and pinhole sizes and wavelengths are given.

From the visibility function calculated, a coupling is derived between parameters specified in the two separated beams. This coupling shows, for example, in what sense a *detector* can be interpreted as a light *source* for the fringe pattern obtained by scanning the other detector, an idea used by Shih *et al.* [3]. The relationship between the coincidence coherence area in the signal beam and the detection area in the idler beam is an aspect of an extended van Cittert–Zernike theorem on fourth-order correlation functions of the electromagnetic field.

II. FOURTH-ORDER CORRELATION FUNCTION

A direct calculation of the fourth-order correlation function $\mathcal{G}^{(4)}$ shows the photon coincidences between the signal and idler beams and generates the entanglement between coherence areas in the conjugated beams:

$$\mathcal{G}^{(4)}=\langle\psi(t)|\hat{E}_s^{(-)}(\mathbf{r}_s,t)\hat{E}_i^{(-)}(\mathbf{r}_i,t+\tau)\times\hat{E}_i^{(+)}(\mathbf{r}_i,t+\tau)\hat{E}_s^{(+)}(\mathbf{r}_s,t)|\psi(t)\rangle. \quad (1)$$

The wave function $|\psi(t)\rangle$ is given by Mandel's theory in the interaction picture [see, for example, Eq. (2) in the work of Ou *et al.* in [6]], $\mathbf{r}_s$ and $\mathbf{r}_i$ specify the positions of the signal and idler detectors, and the electric field operators $\hat{E}_s$ and $\hat{E}_i$ refer to the signal and idler fields at those positions; τ is a time delay between the signal and idler collected photons.

In the experiment performed, $\hat{E}_s^{(+)}(\mathbf{r}_s,t)$ is the sum of the fields on the signal detector coming from the two slits placed in the signal beam path. Writing these field operators as $\hat{E}_j^{(\pm)}(\mathbf{r}_{sj},t_j)$ $(j=1,2)$ the correlation function $\mathcal{G}^{(4)}$ is

$$\mathcal{G}^{(4)}=\langle\hat{E}_1^{(-)}\hat{E}_1^{(+)}\hat{E}_i^{(-)}\hat{E}_i^{(+)}\rangle+\langle\hat{E}_1^{(-)}\hat{E}_2^{(+)}\hat{E}_i^{(-)}\hat{E}_i^{(+)}\rangle+\langle\hat{E}_2^{(-)}\hat{E}_1^{(+)}\hat{E}_i^{(-)}\hat{E}_i^{(+)}\rangle+\langle\hat{E}_2^{(-)}\hat{E}_2^{(+)}\hat{E}_i^{(-)}\hat{E}_i^{(+)}\rangle \quad (2)$$

and the wave function $|\psi(t)\rangle$ is

$$|\psi(t)\rangle=|\psi_{\rm vac}\rangle+\eta\frac{(\delta\omega)^{3/2}}{\sqrt{2\pi}}\sum_{\mathbf{k}_s}\sum_{\mathbf{k}_i}\int_{t-t_{\rm int}}^{t}dt'\,e^{ic(k_s+k_i-k_p)t'}\times\Phi(\mathbf{k}_s,\mathbf{k}_i;\mathbf{k}_p)v(\mathbf{k}_p)|1_{\mathbf{k}_s}\rangle|1_{\mathbf{k}_i}\rangle+\cdots, \quad (3)$$

where $t_{\rm int}$ is the interaction time and

$$\Phi(\mathbf{k}_s,\mathbf{k}_i;\mathbf{k}_p)=\int_V d\mathbf{r}\;\; e^{-i\Delta\mathbf{k}\cdot\mathbf{r}}\prod_{j=1}^{3}\sqrt{\frac{k_j}{k_{0j}}}e^{-(x^2+y^2)/2\sigma_\perp^2}=\sqrt{\frac{k_sk_i}{k_{s0}k_{i0}}}\frac{\sin(\Delta k_z l_z/2)}{(\Delta k_z/2)}\times 2\pi\sigma_\perp^2 e^{-\sigma_\perp^2/2(\Delta k_x^2+\Delta k_y^2)} \quad (4)$$

is the spectral function [11]. $\sigma_\perp$ is the laser beam profile width at the crystal and $\Delta k_\alpha=\Delta\mathbf{k}\cdot\mathbf{e}_\alpha=[\mathbf{k}_s n_s(k_s)+\mathbf{k}_i n_i(k_i)-\mathbf{k}_p n_e(k_p)]\cdot\mathbf{e}_\alpha$. The unit vector $\mathbf{e}_\alpha$ points along a direction α and n_s and n_i are Selmeier's refraction indices for the down-converted beams. In the adopted notation, $k\times n$ means the wave-vector amplitude inside the medium. Type-I down-conversion is chosen due to the simpler angular dependence; the understanding of the field correlations is similar in all cases of spontaneous down-conversion. The k_0's are the magnitudes of central wave vectors specified by the frequency filters.

The parameter η is connected with the efficiency of the down-conversion process [6]

$$\eta\equiv\frac{l^*(\mathbf{k}_{0s})l^*(\mathbf{k}_{0i})l(\mathbf{k}_{0p})}{2\pi i\hbar N(cA)^{3/2}}\tilde{\chi}_{ijk}^{(2)}\times(\mathbf{e}_{\mathbf{k}_3,s_3})_i(\mathbf{e}_{\mathbf{k}_1,s_1})_j^*(\mathbf{e}_{\mathbf{k}_2,s_2})_k^*. \quad (5)$$

In particular, η contains the field amplitudes l, that is to say, the luminescence depends *parametrically* on the field ampli-

[1] A recent tentative explanation by Rehácek and Peřina [10] of the transverse effects was specifically directed to compare the nonlocal control of the visibility degree of the coincidence interference fringes. They utilized Mandel's theory, but kept the spectral function Φ as a constant. A constant Φ is equivalent to the use of *nondiverging* converted beams. However, the transverse correlations seen are intrinsically related to the divergence, and those authors had to impose this divergence *ad hoc*, bypassing the adopted formalism. Furthermore, the experiment [2] was performed scanning the signal beam detector along to the down-converted cone (the small divergence condition), while Ref. [10] assumed the experimental divergence normal to the cone (the strong divergence condition); see Fig. 1.

tudes and on the electrical susceptibility $\chi^{(2)}$. N is the normalization constant [6] for Φ and A is the mode cross section.

As the main focus will be on the transverse properties, the summations indicated are to be performed in the complete set of wave vectors $\{\mathbf{k}\}$ and not just on frequencies. In this case, for each ω a range of wave vectors has to be considered, the very essence of the divergence in a multimode monochromatic theory.

The mathematical problem resides in the calculation of any of the terms in $\mathcal{G}^{(4)}$, for example,

$$\hat{E}_2^{(+)}\hat{E}_i^{(+)}|\psi(t)\rangle. \tag{6}$$

From this term, all others can be obtained by a simple change of indices. The propagating polarized electric-field operator, in vacuum, that reaches a detector is written as

$$\hat{E}^{(+)}(\mathbf{r},t)=-i\sqrt{\frac{c\hbar}{2\epsilon_0 V}}\sum_{\mathbf{k}}\sqrt{k}\hat{a}(\mathbf{k})e^{i(\mathbf{k}\cdot\mathbf{r}-\omega_{\mathbf{k}}t)}F(k), \tag{7}$$

where F (F_s and F_i) are filter functions for the collected light, e.g., Gaussian-like functions centered on k_{0s} and k_{0i} or, simply, monochromatic filters (Dirac δ) in these wave vectors. The term given by Eq. (6) can be explicitly written as

$$\begin{aligned}\hat{E}_2^{(+)}(\mathbf{r}_2,t_2)\hat{E}_i^{(+)}(\mathbf{r}_i,t_2+\tau)|\psi(t)\rangle&\\ =-\eta\frac{c\hbar V\ \delta\omega^{3/2}}{2\epsilon_0(2\pi)^{13/2}}\iint dk_s dk_i e^{ik_s(s_2-ct)}&\\ \times e^{-ik_s c(t+\tau)}\gamma(\mathbf{r}_2,\mathbf{r}_i;k_s,k_i,k_p)(k_s k_i)^{5/2}&\\ \times v_p F_s(k_s)F_i(k_i)\delta(k_s+k_i-k_p)|0_{k_s}\rangle|0_{k_i}\rangle,&\end{aligned} \tag{8}$$

where the Dirac-δ came from the limit of long interaction time t_{int} in Eq. (3) and s_1 and s_2 are the distances between slits 1 and 2 and the signal detector; $t=t_1=t_2$ indicates the time when a photon wave packet reaches the double slit.

The entanglement between signal and idler photons is produced at the crystal source and all spatial (angular) information on the far radiation field is contained in the two-point spectral density function $\gamma(\mathbf{r}_s,\mathbf{r}_i;k_s,k_i)$, defined by

$$\begin{aligned}\gamma(\mathbf{r}_{sj},\mathbf{r}_i;k_s,k_i)\equiv\iint_{\text{radiation field}}d\Omega_s d\Omega_i\ \ \Phi(\mathbf{k}_s,\mathbf{k}_i;\mathbf{k}_p)&\\ \times e^{i\mathbf{k}_s\cdot\mathbf{r}_{sj}}e^{i\mathbf{k}_i\cdot\mathbf{r}_i},&\end{aligned} \tag{9}$$

where $d\Omega_s=d\phi_s d\theta_s\sin\theta_s$ and $d\Omega_i=d\phi_i d\theta_i\sin\theta_i$ are solid angles for the signal and idler wave vectors around the origin at the crystal and $\mathbf{k}_s$ and $\mathbf{k}_i$ are the signal and idler wave vectors. The vector $\mathbf{r}_{sj}$ gives the slit positions $\mathbf{r}_1$ and $\mathbf{r}_2$.

The complexity of the argument in the sinc function in Φ [Eq. (4)] suggests its substitution by a simpler approximate function. A Gaussian is one of the simplest fast decaying function that could be used. A fit of a sinc function to a Gaussian function, giving more weight to points near the origin, leads to

$$\frac{\sin(\Delta k_z l_z/2)}{(\Delta k_z l_z/2)}\simeq e^{-(\sigma_z^2/2)\Delta k_z^2}, \tag{10}$$

where $\sigma_z\simeq 0.460\ l_z$ and l_z is the crystal length along the pump beam.

III. TWO-POINT SPECTRAL FUNCTION

An exact development of all integrals in Eqs. (8) and (9) is a formidable problem in itself. However, solutions using minor simplifications can be obtained. The one adopted here is the development of sinusoidal functions in $\theta_{s,i}$ angles around the values $\theta_{0s,0i}$ of perfect phase matching condition, keeping only terms in first order in $\Delta\theta_{s,i}$. No simplification is made for the sinusoidal functions of ϕ. The leading term for $\gamma(\mathbf{r}_2,\mathbf{r}_i;k_s,k_i)$, for example, is

$$\gamma(\mathbf{r}_2,\mathbf{r}_i;k_s,k_i)=\mathcal{A}' J_0(\mathcal{F}_2), \tag{11}$$

where

$$\begin{aligned}\mathcal{A}'=(2\pi)^{5/2}\sqrt{\frac{k_s k_i}{k_{0s}k_{0i}}}\ l_z\exp(ik_s z_2\cos\theta_{s0}^{\text{ext}})&\\ \times\exp(ik_i z_i\cos\theta_{i0}^{\text{ext}})e^{ik_s(s_2-ct)}e^{-ik_s c(t+\tau)}&\\ \times\left(\frac{u_i}{u_s}+\frac{u_s}{u_i}\right)\frac{\exp\{-[\sigma_\perp k_{s\perp}(n_s-n_i)/\sqrt{2}]^2\}}{k_{s\perp}\sqrt{n_s n_i}}.&\end{aligned} \tag{12}$$

The argument $\mathcal{F}_2$ of the Bessel function J_0 is

$$\mathcal{F}_2=k_{s\perp}n_s\ \sqrt{(x_2-x_i)^2+(y_2-y_i)^2} \tag{13}$$

and the functions u_s and u_i are $u_s=q_s-2\ \theta_{0s}p_s-\theta_{0i}\ r_{si}$ and $u_i=q_i-2\theta_{0i}p_i-\theta_{0s}r_{si}$, with $p_s=n_s^2(\sigma_\perp^2\ k_{sz}^2+\sigma_z^2\ k_{s\perp})$ and $p_i=n_i^2(\sigma_\perp^2\ k_{iz}^2+\sigma_z^2\ k_{i\perp})$, $q_s=2n_s^2\sigma_\perp^2 k_{sz}k_{s\perp}$, $q_i=2n_i^2\sigma_\perp^2 k_{iz}k_{i\perp}$, and $r_{si}=2\ \ n_s^2\ \sigma_z\ k_{s\perp}^2$

The function $\gamma(\mathbf{r}_1,\mathbf{r}_i;k_s,k_i)$ is obtained by exchanging indexes $2\rightarrow 1$. $\mathcal{F}_2$ may be particularized to points near the (y,z) plane for comparison to experimental results (see Fig. 1):

$$\begin{aligned}\mathcal{F}_2=k_{s\perp}n_s[(|y_2|+|y_i|)^2+2\rho\sin\varphi(-x_2+x_c)&\\ +2\rho\cos\varphi\cos\theta_{0i}(|y_2|+y_i)+\rho^2(\sin^2\varphi&\\ +\cos^2\varphi\ \cos^2\theta_{0i})]^{1/2}.&\end{aligned} \tag{14}$$

The variables ρ and φ specify a point within the idler pinhole of radius a, with the origin x_c at the pinhole's center.

IV. MONOCHROMATIC KERNEL

To emphasize the importance of a monochromatic approach, the frequency filters defined in Eq. (8) can be made Dirac-δ-like, with the consequent elimination of the remaining integrals in the wave-vector magnitudes. Collecting all terms that compose a monochromatic ''kernel'' $\mathcal{G}^{(4)}=\mathcal{G}_m^{(4)}$ it is straightforward to arrive at

$$\mathcal{G}_m^{(4)}=|\mathcal{A}|^2\{J_0^2(\mathcal{F}_1)+J_0^2(\mathcal{F}_2)+2\,J_0(\mathcal{F}_1)\;J_0(\mathcal{F}_2)\times\cos[k_{sz}(z_2-z_1)+k_s(s_2-s_1)]\},\tag{15}$$

where $\mathcal{A}=[-c\hbar\,\eta v_p(2\pi cA)^{3/2}/2\epsilon_0 V^{1/2}]\mathcal{A}'$.

The first term in $\mathcal{G}_m^{(4)}$ gives the coincidences between photons reaching the signal detector coming from slit 1 and photons reaching the idler detector, with a similar reasoning for the second term. The last term is the interference between these two possibilities.

In another way, this shows the basic aspect of a high-order interference pattern. While the first term (or the second one) of Eq. (15) shows time coincidences due to the occurrence of a pair of conjugate photons, the third term gives the interference between two possibilities for a given *pair* of photons: One photon of the pair could be coming to the signal slit 1 and the second photon of the pair to the idler detector, or these photons could be coming to signal slit 2 and to the idler detector. The *indistinguishability* of these two possibilities, due to *transverse* correlations, brings the high-order interference term into play.

V. VISIBILITY

In order to obtain an expression from the kernel $\mathcal{G}_m^{(4)}$ to be compared with experimental results, integrations have to be performed in Eq. (15) over the idler-pinhole (radius a) and signal-slit areas (width δ), leading to

$$\mathcal{G}_{m-\mathrm{expt}}^{(4)}\simeq\frac{|\mathcal{A}|^2}{\pi k_{s\perp}n_s(|y_2|+|y_{ic}|)}\times\left[1+2\frac{J_1(adk_{s\perp}n_s/(|y_2|+|y_{ic}|))}{(adk_{s\perp}n_s/(|y_2|+|y_{ic}|))}\right]\times\cos\left(\frac{x_c dk_{s\perp}n_s}{(|y_2|+|y_{ic}|)}\right)\cos\left(\frac{xdk_s}{L}\right)\times\left(\frac{\sin\left(\frac{x\delta\,k_s}{4L}\right)}{\left(\frac{x\delta k_s}{4L}\right)}\right)^2\Bigg].\tag{16}$$

Similarly, to consider a finite a size h for the signal detector, an integration, leading to an analytic result, can be performed on x', writing $x\to x+x'$ in the above expression. Each integral has to be properly normalized by the involved length.

A direct examination of the expression $\mathcal{G}_{m-\mathrm{expt}}^{(4)}$ shows that the *object* interference can be measured by scanning the x variable (signal detector position) and the conjugate *image* appears scanning x_c (idler pinhole-detector system x position) with a fixed idler $y(=y_{ic})$ central position.

Besides direct comparisons between coincidence spectra predicted by this function and experimental results, quite stringent comparisons can be done through the visibility degree $v^{(4)}$ obtained from the *coincidence* fringe patterns. This is a very sensible function with respect to all relevant parameters in the problem. For example, for an object pattern seen when $x_c=0$ and the signal detector is pointlike, the visibility $v^{(4)}$ is

$$v^{(4)}=2\frac{J_1(adk_{s\perp}n_s/(|y_2|+|y_{ic}|))}{adk_{s\perp}n_s/(|y_2|+|y_{ic}|)},\tag{17}$$

where J_1 is a Bessel function. Similarly, if the finite size of the signal detector is taken into account, the visibility $v^{(4)}=v_s^{(4)}$ can be calculated using a single point x, $x=0$, for example, with the result

$$v_s^{(4)}=2\frac{J_1(adk_{s\perp}n_s/(|y_2|+|y_{ic}|))}{adk_{s\perp}n_s/(|y_2|+|y_{ic}|)}\left(\frac{4L}{\delta hk_s}\right)^2[-2\,{}_2F_1(\mathcal{D})+{}_2F_1(\mathcal{D}_+)+{}_2F_1(\mathcal{D}_-)],\tag{18}$$

where ${}_2F_1$ is a Gauss hypergeometric function,

$$\mathcal{D}=\left\{-\frac{1}{2},\left(\frac{1}{2},\frac{1}{2}\right),-\left(\frac{dhk_s}{4L}\right)^2\right\},$$

$$\mathcal{D}_+=\left\{-\frac{1}{2},\left(\frac{1}{2},\frac{1}{2}\right),-\left(\frac{(2d+\delta)hk_s^2}{8L}\right)^2\right\},$$

and

$$\mathcal{D}_-=\left\{-\frac{1}{2},\left(\frac{1}{2},\frac{1}{2}\right),-\left(\frac{(2d-\delta)hk_s}{8L}\right)^2\right\}.$$

VI. ENTANGLED COHERENCE AREAS

In Ref. [2], Ribeiro *et al.* pointed out that the experimental results indicate an entanglement of coherence areas between the signal coherence area on the double-slit location and the idler pinhole area. This entanglement is now written as an aspect of a higher-order extension of the van Cittert–Zernike theorem. The first zero z_0 of the J_1 Bessel function in the visibility $v^{(4)}$, $z_0\simeq 3.831\,71$, gives

$$ad=z_0\frac{|y_2|+|y_{ic}|}{k_{s\perp}\,n_s}.\tag{19}$$

Taking d_c^2 as the signal coherence area

$$d_c^2=\left(z_0\frac{r_{s2\perp}+r_{i\perp}}{(k_{s\perp}n_s)a}\right)^2,\tag{20}$$

shows in what sense the idler detector area πa^2, for example, could be interpreted as a ''source'' for the slit fringe pattern. Here $r_{s2\perp}=|y_2|=r_{s1\perp}$ and $r_{i\perp}=|y_{ic}|$. In degenerate cases, $\theta_{0s}=\theta_{0i}$ and

$$d_c^2=\left(z_0\frac{r_{sj}+r_i}{k_s\,n_s a}\right)^2,\tag{21}$$

in agreement with the dependence on $r_{sj}+r_i$ pointed in Ref. [3].

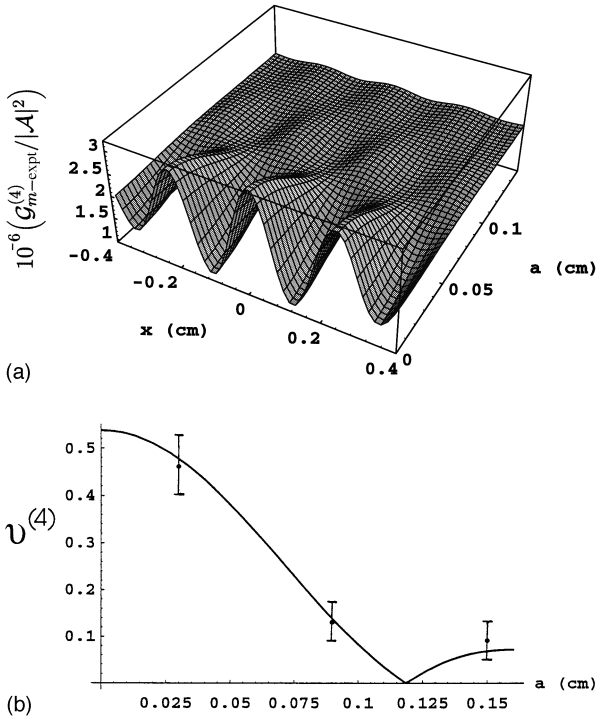

FIG. 2. (a) Fourth-order correlation function $\mathcal{G}^{(4)}_{m\text{-expt}}/|\mathcal{A}|^2\times10^6$ (dimensionless) as a function of the signal detector position x and the idler pinhole radius a. (b) Object visibility degree $|v_s^{(4)}|$ as a function of the idler pinhole size a. $r_i=50$ cm, $r_s=2$ cm, $L=45$ cm, $x_c=0$ cm, $k_s=7.9665\times10^4$ cm^{-1}, $k_i=9.9292\times10^4$ cm^{-1}, and $k_p=1.7896\times10^5$ cm^{-1}.

Equations (19) and (20), derived from the visibility $v^{(4)}$, show the effect of a finite-size idler detector of area πa^2 on the signal coherence area represented by d_c^2 This relationship expresses the extraordinary fact that the crystal-to-slit distance r_{sj} does not determine the visibility of the interference patterns as in the classical van Cittert–Zernike theorem but that it depends on $r_{sj}+r_i$. Therefore, the double slit may present fourth-order interference even when no second-order interference exists.

This result is also consistent with the idea presented in Ref. [3] for a parallel pump laser beam, showing that the crystal acts as a mirror if one is using point size detectors. The finite detector sizes now analyzed extends that idea and furnishes the principles of a two-photon physical optics. This *two-photon physical optics* will certainly be necessary, for example, in the design of equipment relying on transverse correlations of twin photons.

VII. EXPERIMENTAL COMPARISONS

A main experimental result in Ref. [2] is the demonstration of the nonlocal *contrast* control of the signal object fringe by variation of the idler pinhole size. Without fitting parameters, the calculated degree of visibility $v_s^{(4)}$ is shown in Fig. 2 together with the experimental points obtained by fitting the interference fringes to a first order-like interference pattern as described in [2]. The agreement is within experimental errors. The theoretical prediction shows a structure with minima that can be experimentally explored.

Another striking data from Ref. [2] is the very slow variation of $v_s^{(4)}$, obtained from the object fringe, with the crystal-to-slits distance r_s. A plot of $\mathcal{G}^{(4)}_{m\text{-expt}}$ as a function of the distance r_s shows, in Fig. 3, the slow increase of $v_s^{(4)}$ with r_s. There is a slight decrease in coincidence counts with increasing r_s. The parameters were kept the same as the ones in Fig. 2 except r_s. The visibility degree predicted is within 10% of the experimental values.

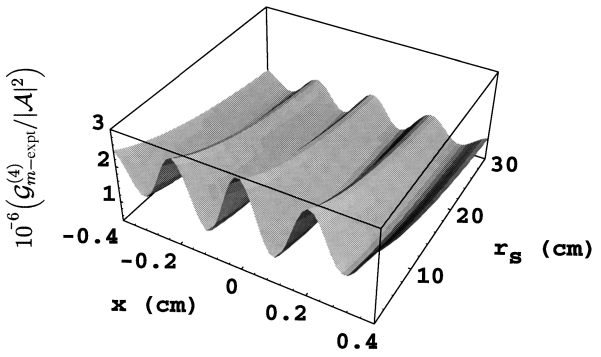

FIG. 3. Fourth-order correlation function $\mathcal{G}^{(4)}_{m\text{-expt}}/|\mathcal{A}|^2\times10^6$ (dimensionless) as a function of the signal detector position x and the crystal to slits distance r_s. There is a slow increase of the visibility degree with r_s, while the coincidence intensity slowly decreases.

The fourth-order correlation function $\mathcal{G}^{(4)}_{m\text{-expt}}$ Eq. (16), predicts the dependence on x, the signal detector position, and on x_c, the idler pinhole-detector position. Figure 4 shows the correlation between object and ''image'' fringes. Parameters used in this plot were taken from the experimental conditions specified in our laboratory.

Figure 5 shows the experimental visibilities (dots) obtained for image patterns in function of the signal detector ''size'' h [12], fitted with a classical *second-order* visibility function [13]. The signal detector size h is simulated by a variable pinhole and lens system placed after the double slit. The detector is placed at the focal plane of the lens, collecting almost all light passing through the pinhole. The predicted visibility $v_s^{(4)}$ (solid line) is compared with the obtained fit. Again, the theory suggests that the existence of features in the coincidence visibility should be experimentally tested.

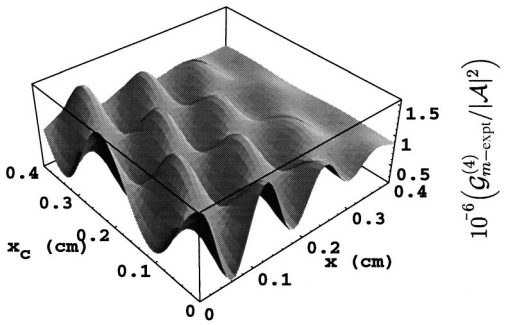

FIG. 4. Fourth-order correlation function $\mathcal{G}^{(4)}_{m\text{-expt}}/|\mathcal{A}|^2\times10^6$ (dimensionless) as a function of x (object fringe) and x_c (image fringe). $r_i=50$ cm, $r_s=10$ cm, $L=26$ cm, $a=0.05$ cm^{-1}, and $h\simeq0.01$ cm^{-1}. $k_s=7.9665\times10^4$ cm^{-1}, $k_i=9.9292\times10^4$ cm^{-1}, and $k_p=1.7896\times10^5$ cm^{-1}.

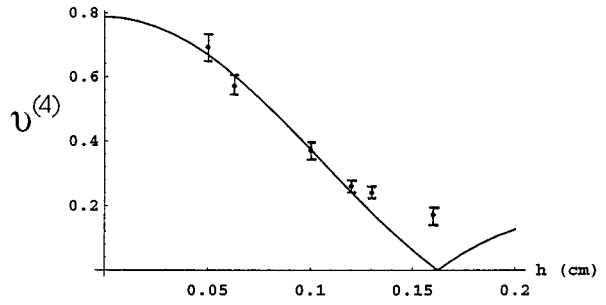

FIG. 5. Comparison between the degree of visibility obtained experimentally from image fringes and the theoretical prediction from $|\upsilon_s^{(4)}|$, as the signal detector ''size'' is varied; all other parameters from Fig. 4 were used.

The final theoretical results presented in this work for $\upsilon^{(4)}$ and the complete dependence on parameters in $\mathcal{G}^{(4)}$ were developed within a monochromatic framework with the aim of showing the main features of the theory and the basic agreement with the data. Although this has been achieved, explaining all the basic dependences experimentally seen, one should keep in mind that the data were taken with a finite bandwidth filter. For example, Figs. 2(b) and 5 compare predictions from the visibility $\upsilon^{(4)}$ to the data obtained by fitting the interference fringes to a first-order-like interference pattern as discussed in Refs. [2,13]. However, it is intuitive that the superposition of curves of $\upsilon^{(4)}$ with different zeros of the Bessel function, due to different wavelengths, would lead to the smearing of the zero produced by a monochromatic theory. This lack of a defined zero is clearly seen in Fig. 5.

VIII. CONCLUSIONS

Applying the basic theory developed by Mandel and coworkers, this work explores the function $\mathcal{G}^{(4)}$ in the $\{\mathbf{r}\}$ space, summing over the whole set of wave vectors $\{\mathbf{k}\}$. Particularized to a multimode monochromatic solution, analytic expressions for $\mathcal{G}^{(4)}_{m\text{-expt}}$ and $\upsilon_s^{(4)}$ are obtained and compared satisfactorily with experimental results for the whole range of variable parameters.

The entanglement between signal and idler coherence areas shown by the visibility function $\upsilon^{(4)}$ [Eq. (19)] is an aspect of an extended van Cittert–Zernike theorem for coincidence experiments. One of the conclusions derived in this work, for degenerate down-conversion, is that the effective distance between the fictitious source and the conjugate detector is $r_{sj}+r_i$, justifying the unexpected behavior pointed out in [3]. The effort by many authors to study the down-conversion luminescence has enriched our knowledge of this remarkable phenomenon, where several tests of quantum mechanics have been performed, and the incipient studies of transverse correlations of this light field indicate a fertile ground to be explored.

ACKNOWLEDGMENTS

This work was supported by the Brazilian research funding agencies CNPq, FINEP, and FAPEMIG. Dr. P. H. Souto Ribeiro is acknowledged for his insight on the importance of the angular divergence $(\hat{\mathbf{k}})$ in these problems. Thanks are due to Dr. S. Pádua and Dr. C. H. Monken for a critical reading of the manuscript.

[1] D. C. Burham and D. L. Weinberg, Phys. Rev. Lett. **25**, 84 (1970); W. H. Louisell, A. Yariv, and A. E. Siegman, Phys. Rev. **124**, 1646 (1961); D. Magde and H. Mahr, *ibid.* **171**, 393 (1968); G. T. Giallorenzi and C. L. Tang, *ibid.* **166**, 225 (1968); B. Ya. Zel'dovich and D. N. Klyshko, Pis'ma Zh. Éksp. Teor. Fiz. **9**, 69 (1969) [JETP Lett. **9**, 40 (1969)].

[2] P. H. S. Ribeiro, S. Pádua, J. C. Machado da Silva, and G. A. Barbosa, Phys. Rev. A **49**, 4176 (1994).

[3] Y. H. Shih, A. V. Sergienko, T. B. Pittman, D. V. Strekalov, and D. N. Klyshko, Ann. N. Y. Acad. Sci. **755**, 121 (1995); D. V. Strekalov, A. V. Sergienko, D. N. Klyshko, and Y. H. Shih, Phys. Rev. Lett. **74**, 3600 (1995).

[4] C. H. Bennett and S. J. Wiesner, Phys. Rev. Lett. **69**, 2881 (1992); S. Popescu, *ibid.* **72**, 797 (1994).

[5] A. Einstein, B. Podolsky, and N. Rosen, Phys. Rev. **47**, 777 (1935).

[6] L. J. Wang, X. Y. Zou, and L. Mandel, Phys. Rev. A **44**, 4614 (1991); X. Y. Zou, L. J. Wang, and L. Mandel, Phys. Rev. Lett. **67**, 318 (1991); Z. Y. Ou, L. J. Wang, and L. Mandel, Phys. Rev. A **40**, 1428 (1989); C. K. Hong and L. Mandel, Phys. Rev. Lett. **56**, 58 (1986).

[7] T. Grayson and G.A. Barbosa, Phys. Rev. A **49**, 2948 (1994).

[8] G. A. Barbosa, Phys. Rev. A **48**, 4730 (1993); **50**, 3379 (1994).

[9] A. Joobeur, B. E. A. Saleh, and M. C. Teich, Phys. Rev. A **50**, 3349 (1994).

[10] J. Rehácek and J. Peřina, in *Proceedings of the Seventh Rochester Conference on Coherence and Quantum Optics*, edited by J. H. Eberly, L. Mandel, and E. Wolf (Plenum, New York, 1996).

[11] X.Y. Zou, T. Grayson, G.A. Barbosa, and L. Mandel, Phys. Rev. A **47**, 2293 (1993).

[12] P. H. S. Ribeiro and G. A. Barbosa, Phys. Rev. A (to be published).

[13] P. H. S. Ribeiro, C. H. Monken, and G. A. Barbosa, Appl. Opt. **33**, 352 (1994).